NANO LETTERS

Letter

pubs.acs.org/NanoLett

An Ultrafast Switchable Terahertz Polarization Modulator Based on III−V Semiconductor Nanowires

Sarwat A. Baig,[†,⊥] Jessica L. Boland,[‡,⊥] Djamshid A. Damry,[‡] H. Hoe Tan,[§] Chennupati Jagadish,[§] Hannah J. Joyce,[*,†] and Michael B. Johnston[*,‡]

[†]Department of Engineering, University of Cambridge, 9 JJ Thomson Avenue, Cambridge CB3 0FA, United Kingdom

[‡]Department of Physics, Clarendon Laboratory, University of Oxford, Parks Road, Oxford, OX1 3PU, United Kingdom

[§]Department of Electronic Materials Engineering, Research School of Physics and Engineering, Australian National University, Canberra, Australian Capital Territory 2601, Australia

S *Supporting Information*

ABSTRACT: Progress in the terahertz (THz) region of the electromagnetic spectrum is undergoing major advances, with advanced THz sources and detectors being developed at a rapid pace. Yet, ultrafast THz communication is still to be realized, owing to the lack of practical and effective THz modulators. Here, we present a novel ultrafast active THz polarization modulator based on GaAs semiconductor nanowires arranged in a wire-grid configuration. We utilize an optical pump−terahertz probe spectroscopy system and vary the polarization of the optical pump beam to demonstrate ultrafast THz modulation with a switching time of less than 5 ps and a modulation depth of −8 dB. We achieve an extinction of over 13% and a dynamic range of −9 dB, comparable to microsecond-switchable graphene- and metamaterial-based THz modulators, and surpassing the performance of optically switchable carbon nanotube THz polarizers. We show a broad bandwidth for THz modulation between 0.1 and 4 THz. Thus, this work presents the first THz modulator which combines not only a large modulation depth but also a broad bandwidth and picosecond time resolution for THz intensity and phase modulation, making it an ideal candidate for ultrafast THz communication.

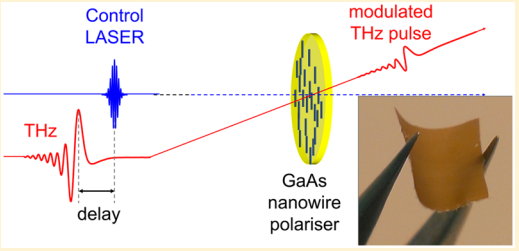

KEYWORDS: *Terahertz (THz), GaAs, nanowire, parylene, polarizer, modulator*

Terahertz (THz) radiation, lying between the infrared and microwave regions of the electromagnetic spectrum, has historically been an elusive frequency range (0.1−10 THz) with THz technology in its infancy.[1] Yet, the THz range has come into the limelight due to its enormous promise in a variety of applications, such as in biological and medical sciences, nondestructive evaluation, security, and ultrafast computing.[2,3] Initial progress in the field was hampered by a lack of intense sources of THz radiation,[4,5] but in the past 20 years huge advances have been made in THz generation[6−12] and detection.[1,13−17] These advances have enabled the development of THz time-domain spectroscopy for in-depth material characterization,[18−22] as well as noninvasive THz imaging for medical applications.[23,24] Despite these significant developments, one application that has still not been realized is high-speed THz communication. In order to achieve this, active THz components that can directly manipulate and process THz radiation are essential.

At present, the development of practical effective THz modulators is an active field of research with many different approaches being investigated. Depending on which property of light is controlled, THz modulators can come in different forms, with information encoded on the THz wave by modulating the intensity,[25,26] phase,[27,28] or spatial position of the transmission and reflection coefficients of the THz electric field.[29,30] Previous works have mainly focused on modulation of THz intensity, with early demonstrations based on two-dimensional electron-gas (2DEG) structures,[31,32] birefringent liquid crystals,[33,34] and static THz polarizers.[35−38] Recently, THz modulation has also been realized with metamaterials,[25,27,29,37,39−43] optical cavities,[44,45] graphene,[46−49] and carbon nanotubes,[28,50,51] each with their own merits and weaknesses.

Metamaterial-based THz modulators have achieved high modulation depths, with Karl et al.[52] demonstrating a dynamic range of over 20 dB and Chen et al. showing a modulation depth of ∼50%.[39,53] However, these THz modulators suffer from low bandwidth, with optimal operation only at a designed wavelength, as well as limited switching speeds with microsecond temporal resolution. THz amplitude modulators based on Fabry−Perot semiconductor cavity designs have also been demonstrated, with a modulation depth of ∼90%, yet only microsecond switching speeds.[45] Recently, Liu et al. have demonstrated THz modulation with close to 100% modulation

Received: January 29, 2017
Revised: March 16, 2017
Published: March 23, 2017

DOI: 10.1021/acs.nanolett.7b00401
Nano Lett. 2017, 17, 2603−2610

depth by utilizing the evanescent wave in a total internal reflection setup coupled with a conductive interface to enhance attenuation of THz radiation.[54] This technique offers flexibility in terms of the choice of material used to produce the modulator as only low sheet conductivities on the order of 12 mS are required to obtain a high modulation depth, and the broadband response is purely dictated by the frequency-dependent conductivity response of the material. Similarly, the switching speed is also determined by the material response and therefore could be improved through careful choice of the THz modulator material.

With the aim of improving switching speeds, graphene-based modulators have been shown to improve performance, by utilizing intraband absorption to obtain a modulation depth of ∼16% and nanosecond modulation time.[46] By utilizing a total internal reflection geometry, the modulation depth of these graphene-based modulators could be improved up to 70% per reflection.[55] Furthermore, carbon-nanotube based THz polarizers have been demonstrated. Ren et al.[50] fabricated static carbon nanotube THz polarizers by depositing aligned nanotubes onto a sapphire substrate and reported an extinction ratio of 10 dB in the optical and THz range, whereas Kyoung et al.[51] demonstrated an extinction ratio of 37 dB by using a carbon nanotube stack fabricated from aligned nanotube arrays to produce static THz polarizers. However, in order to realize ultrafast THz communication, modulation times on the order of picoseconds are required. Carbon nanotube−polymer based modulators can offer such high switching speeds, yet at the cost of modulaton depth. Docherty et al.[28] demonstrated an ultrafast switchable carbon nanotube THz polarizer, which could be optically controlled and was capable of polarization and intensity modulation of THz radiation with a time resolution on the order of 1 ps, although it suffered from a low modulation depth of around −27 dB. Thus, there is still a need for the development of a practical THz modulator with a high modulation depth and picosecond switching speeds, which can be electrically or optically controlled and can be easily integrated into current silicon-based technology.

Here, we present the first THz intensity and polarization modulator based on III−V semiconductor nanowires that provides both picosecond switching speeds and high modulation depth. III−V nanowires are of particular interest for use in THz applications due to their high electron mobilities and their ability to be integrated with silicon devices.[56] In particular, GaAs nanowires are ideal candidates for THz modulation, as they exhibit a direct bandgap, high absorption coefficient, and tunable optoelectronic properties, such as carrier lifetimes and mobility.[19,57] They are rendered conductive in the THz region upon photoexcitation, absorbing THz radiation polarized parallel to the long axis of the nanowire and thereby reducing THz transmission.[58] Thus, they can offer a practical, cost-effective alternative to other THz modulation techniques, while providing a system that can not only modulate the intensity of the THz radiation but also the polarization. This allows for an increase in information that can be encoded on the THz wave and the realization of high-speed THz communication.

In this Letter, we demonstrate THz nanowire polarizers fabricated from aligned GaAs nanowires embedded in a parylene C membrane. We characterize their optoelectronic properties via optical pump−terahertz probe (OPTP) spectroscopy, showing a photoconductivity lifetime of approximately 1 ps for the GaAs nanowires. This short lifetime allows for subpicosecond switching speeds, even faster than those demonstrated by carbon nanotube polarizers. We also observe a significant photoinduced change in THz transmission between 0.1 and 4 THz, enabling a large bandwidth for THz modulation that exceeds values previous seen for other THz modulators. We demonstrate THz modulation by changing the polarization of photoexcitation of the nanowires and show an extinction of 13.5%, modulation depth of −8 dB, and dynamic range of −9 dB in THz transmission, comparable to those achieved by graphene-based THz modulators and far surpassing those seen for optically activated carbon nanotube THz polarizers.

For our THz modulator, we have selected GaAs nanowires as the active modulating elements due to their properties of (i) high, anisotropic THz conductivity when photoexcited and (ii) short photoconductivity lifetime of less than 5 ps. These properties together should enable the modulation of THz transmission on ultrafast time scales.[59] High-density arrays of ⟨111⟩B-oriented GaAs nanowires of diameter 50 nm were grown via gold-seeded metalorganic chemical vapor deposition (MOCVD) on GaAs (100) substrates. Figure 1a shows a plan-

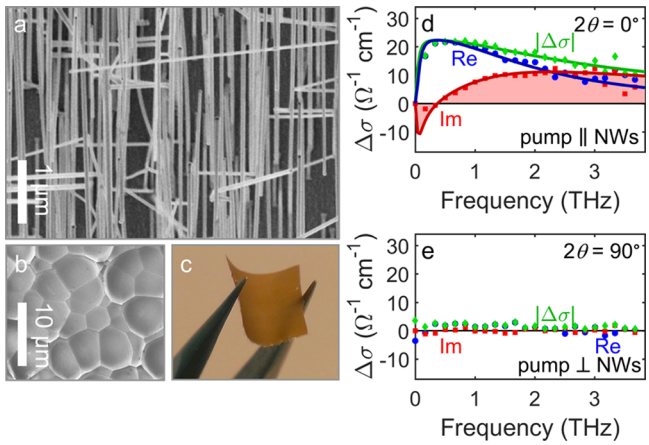

Figure 1. (a) SEM image of ⟨111⟩B-oriented GaAs nanowires grown on the GaAs ⟨100⟩ substrate before they are embedded in parylene. (b) SEM image of the top of a 5-μm-thick parylene layer in which aligned GaAs nanowires are embedded. (c) Photograph of a polarizer consisting of nanowires encapsulated in a single layer of parylene. (d, e) Frequency-dependent photoconductivity response of nanowires after photoexcitation with the pump pulse polarized (d) parallel to the nanowire axis and (e) perpendicular to the nanowire axis. Blue circles, red squares, and green diamonds represent the real part, imaginary part, and magnitude of the photoconductivity, respectively. Lines represent fits to the conductivity modeled by a Drude−plasmon response.

view scanning electron microscope (SEM) image of the GaAs nanowires grown on these substrates. The nanowires are well aligned with most pointing in the ⟨111⟩B directions. Thus they point at a shallow angle of 35.3° to the plane of the (100) wafer, so may be thought of as lying almost flat on the GaAs substrate. Further details of the sample geometry can be found in the Supporting Information (SI, Section 1.2 and Figure S1). The nanowires were grown via a two-temperature process that gives high uniformity in nanowire diameter, a twin-free zinc-blende structure, and high charge carrier mobilities.[59,60]

The GaAs nanowire wafers were then coated with a 5 μm layer of parylene C using the Gorham process[61] in a PSD 2010 LabCoter2 chamber. The highly conformal nature of the parylene C coating ensures the voids between the nanowires

DOI: 10.1021/acs.nanolett.7b00401
Nano Lett. 2017, 17, 2603−2610

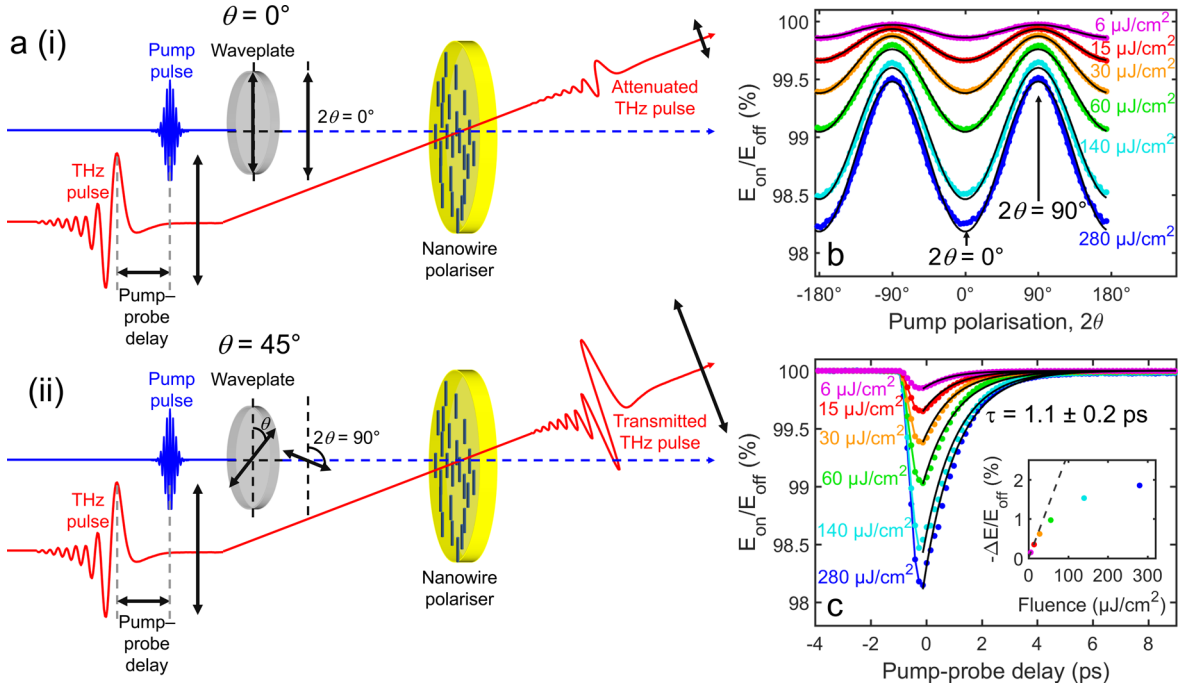

Figure 2. (a) Schematic diagrams of the experiment. The nanowires are oriented vertically, and the incident THz electric field is vertically polarized. The pump beam selectively photoexcites nanowires that are aligned with their long axes parallel to the polarization of the pump beam. The THz pulse is then absorbed by the photoexcited nanowires. (i) When $2\theta = 0°$ the nanowires are aligned with the polarization of the pump beam, so are photoexcited and rendered conductive, leading to maximum THz absorption. (ii) When $2\theta = 90°$ the nanowires are orthogonal to the polarization of the pump beam, so the incident pump pulse does not photoexcite the nanowires effectively, leading to minimum THz absorption. (b, c) Modulation properties of a single layer of aligned GaAs nanowires embedded in parylene C. Photoexcitation was performed with pump fluences between 6 and 280 μJ cm^{-2}. (b) THz transmission, E_{on}/E_{off}, as a function of pump polarization angle (2θ), measured with the pump–probe delay at $t = 0$ ps. Solid black lines represent squared-cosine fits according to Malus' law. (c) THz transmission, E_{on}/E_{off}, as a function of time after photoexcitation, measured with the pump polarized at $2\theta = 0°$. Solid black lines are fits describing monoexponential decay of the photoconductivity at early times after photoexcitation. The inset in panel c plots the modulation depth ($-\Delta E/E_{off}$ measured at $t = 0$ ps and $2\theta = 0°$) as a function of pump fluence. The dashed line in the inset shows the expected values if photoconductivity scaled linearly with pump fluence.

are filled, hence providing excellent encapsulation for the nanowires. Parylene C is also robust, flexible, simple to manufacture, and highly transparent to THz radiation with a low THz refractive index of 1.6,[62] making parylene particularly suitable as a host medium for the photoconductive GaAs nanowires. Figure 1b shows a plan-view SEM image of the 5-μm-thick parylene layer with aligned GaAs nanowires embedded within. Blank microscope slides were also coated in the same way, to provide parylene layers without nanowires as reference samples. The parylene layers encapsulating the nanowires were peeled off from the substrate, and these films were divided into equal sized segments using a razor blade to form 10 mm × 10 mm squares (Figure 1c). To increase modulation depth, multiple layer samples were created to increase the effective areal nanowire density and therefore increase the THz absorption. The thin film layers of nanowires-in-parylene C were laminated together while preserving the alignment of the nanowires. The layers were subsequently hot-bonded together at 120 °C and 20 bar using an Obducat nanoimprinter, to eliminate any air gaps between layers which would otherwise reduce the optical quality of the films. Nanowire polarizers consisting of 1, 4, 8, and 14 layers were fabricated and characterized.

To assess the potential of these parylene-coated GaAs nanowire polarizers for THz modulation, their photoconductivity and THz transmission were measured via OPTP spectroscopy. A Ti:sapphire regenerative amplifier laser with pulse duration of 35 fs, 5 kHz repetition rate, and center wavelength of 800 nm ($h\nu$ = 1.55 eV) was used as a source for both THz generation and detection and optical photoexcitation of the polarizer. The laser pulse was divided into three beams: the first to photoexcite the nanowire polarizers with a beam width of 5 mm at a range of fluences up to 280 μJ cm^{-2}; the second to generate the THz probe beam by optical rectification in a 2 mm ⟨110⟩ GaP crystal, giving a THz beam width of less than 1 mm at the nanowire film; and the third to act as a gate beam for electro-optical sampling of the THz field via a 200 μm ⟨110⟩ GaP crystal. The transmission of the electric field of the THz probe pulse through the nanowires, E, can then be measured as a function of frequency. The electric field transmitted through the sample without photoexcitation (at equilibrium) is given by E_{off}. Upon photoexcitation, free charge carriers are generated in the nanowires, and these carriers interact with the THz wave to reduce the transmission to E_{on}. The photoinduced change in THz transmission through the nanowires is denoted as $\Delta E = E_{on} - E_{off}$. The value of $-\Delta E/E_{off}$ is then proportional to the photoinduced conductivity of the nanowires (see SI) and directly related to the photoexcited free carrier concentration. For convenience, we define $t = 0$ to be the pump–probe delay at which $-\Delta E/E_{off}$ is maximum.[58]

In this OPTP system, the polarization of the photoexcitation beam is selected via a halfwave plate. Figure 2 shows a schematic diagram of the experimental setup, with the cases for $\theta = 0°$ and $\theta = 45°$ depicted. By rotating the halfwave plate by an angle of θ, the polarization of the optical pump beam was altered by an angle of 2θ. Thus, by rotating the halfwave plate

DOI: 10.1021/acs.nanolett.7b00401
Nano Lett. 2017, 17, 2603−2610

by 45°, the optical pump beam was rotated from vertical polarization to horizontal polarization. The nanowires-in-parylene films were placed in the OPTP system, such that the long axes of the constituent nanowires were oriented vertically.

It is the inherent geometric anisotropy of semiconductor nanowires that enables polarized photoexcitation to induce transient modulation of the polarization and intensity of the transmitted THz pulse. Specifically, the dielectric mismatch between the nanowire and the surrounding parylene medium allows an electric field to penetrate the nanowire if the field is polarized parallel to the nanowire axis but strongly suppresses penetration of electric field components oriented perpendicular to the nanowire axis.[63] As a result, nanowires exhibit strong linear polarization anisotropy in response to photoexcitation. Photoexcitation is most effective if the optical pump is polarized parallel to the nanowire axis, but minimally effective if the pump is polarized perpendicular to the nanowire axis. The absorption of THz radiation also strongly depends on the polarization of the THz pulse relative to the nanowire orientation. The plasmon modes that propagate longitudinally along the nanowire axis are responsible for plasmonic THz absorption signatures between 0.1 and 4 THz: these modes strongly absorb components of the THz electric field parallel to the nanowire axis.[58] In all experiments reported here, the THz pulse was polarized parallel to the nanowire axes, which is the configuration that gives the strongest absorption, and therefore modulation, of the THz pulse in the range of 0.1−4 THz.

Without photoexcitation (at equilibrium), there are relatively few charge carriers within the nanowires to absorb the THz radiation. The equilibrium carrier density in the GaAs nanowires was determined previously to be lower than 10^{15} cm^{-3}.[57] Therefore, without photoexcitation, the THz radiation is transmitted with minimal attenuation and retaining its original polarization. Under photoexcitation, nanowires with their long axes aligned parallel ($2\theta = 0°$) to the polarization of the optical pump beam are preferentially excited and contribute to THz conductivity along the nanowire axis.[63] The photoexcited electrons then strongly absorb the component of the THz wave that is polarized parallel to the long axis of the nanowires, so the transmission of this component is attenuated strongly. In contrast, any component of the THz pulse that is polarized perpendicular to the nanowire axis will be transmitted with minimal photoinduced modulation. As 2θ increases to 90°, the optical pump beam polarization becomes orthogonal to the nanowires, and only a minimal density of free charge carriers are photogenerated in the nanowires. Consequently, when $2\theta = 90°$ the THz radiation is barely attenuated, regardless of the polarization of the incident THz radiation. Therefore, by controlling the polarization of the incident optical pump beam, it is possible to modulate the intensity and polarization of the THz wave passing through the nanowire sample.

Figure 1d and e respectively plot the photoconductivity response of the nanowires embedded in parylene C, when the pump beam is polarized parallel and perpendicular to the nanowires. The photoconductivity response is greatest when the pump is polarized parallel to the nanowires and negligible when the pump is polarized perpendicular to the nanowires. The photoconductivity response in Figure 1d exhibits a Lorentzian line shape characteristic of a plasmon response. Fitting a Drude−plasmon response (see SI) to the data in Figure 1d reveals a high electron mobility of 1800 cm^2 V^{-1} s^{-1}, indicative of the excellent electronic properties of the nanowires. The magnitude of the photoconductivity ($\Delta\sigma$) is significant and extends across the measurement bandwidth (0.1 to 4 THz). The broad spectrum of the photoconductivity response of the nanowire−parylene layer indicates its potential as a broadband THz polarizer.

We first assess the transient modulation of THz transmission through the single parylene-coated GaAs nanowire layer. To investigate the effect of the polarization of the optical pump beam on the THz modulation, the ratio of the transmission under photoexcitation to the transmission at equilibrium, $E_{on}/E_{off} = 1 + \Delta E/E_{off}$, is plotted as a function of polarization angle, 2θ, in Figure 2b. This experiment was performed at a range of photoexcitation fluences up to 280 μJ cm^{-2}. Fits to the data show a cosine-squared relationship between the THz transmission and 2θ, as expected from Malus' law for transmission through a polarizer. At $2\theta = 0°$ and $2\theta = \pm 180°$, when the polarization of the optical pump beam is aligned parallel to the nanowire axis, a minimum in the THz transmission (maximum THz absorption) is observed. As the polarization angle is rotated, the THz transmission increases to reach a maximum at $2\theta = \pm 90°$ when the optical pump beam is polarized transverse to the nanowire axis. Thus, to quantify the performance of the ultrafast polarizer, we calculate its modulation depth and dynamic range. We define the modulation depth as the value of $-\Delta E/E_{off}$ reached when the pump is polarized parallel to the nanowires ($2\theta = 0°$). We define the dynamic range as the relative difference in THz transmission when the pump is polarized at angles of $2\theta = 90°$ and $2\theta = 0°$. For this single-layer parylene-coated GaAs nanowire polarizer at the highest investigated fluence (280 μJ cm^{-2}), the modulation depth was found to be -17.4 ± 0.1 dB corresponding to extinction of $\sim 1.82 \pm 0.04\%$, and the dynamic range was determined as -18.8 ± 0.1 dB. These values already exceed values measured for carbon nanotube-based THz polarizers but are not yet ideal for THz modulation in high-speed communication systems. We will later show that, by laminating multiple layers of these nanowires embedded in the flexible thin parylene C host matrix, multilayer nanowire polarizers can be constructed to increase the modulation depth and thereby create more efficient THz modulation.

The switching speed of the GaAs polarizer was determined by measuring the THz transmission as a function of time after photoexcitation at a range of fluences between 6 and 280 μJ cm^{-2}, as shown in Figure 2c. For all fluences, a sharp rise in photoconductivity within 1 ps was observed followed by a rapid decay attributed to trapping of free carriers at the GaAs nanowire surface. A monoexponential function was fitted to the decays over the first 5 ps, from which the photoconductivity decay lifetime extracted. The photoconductivity lifetime was found to be of the order of a picosecond, 1.1 ± 0.2 ps, with the initial photoconductivity, which is related to modulation depth, increasing with fluence. Thus, the GaAs nanowires show great potential for a large modulation in THz transmission with picosecond modulation times through optical switching.

The inset of Figure 2c illustrates that the maximum photoinduced change in transmission, $-\Delta E/E_{off}$, increases only sublinearly with photoexcitation fluence and saturates toward the highest fluences. This phenomenon arises due to two effects that limit the photoconductivity of the GaAs nanowires and therefore limits THz absorption by the nanowires. First, as photoexcitation fluence increases, the charge-carrier density increases, and carrier−carrier scattering mechanisms become more pronounced. This additional

DOI: 10.1021/acs.nanolett.7b00401
Nano Lett. 2017, 17, 2603−2610

scattering reduces the charge carrier mobility and consequently limits the photoconductivity of the nanowires at the highest fluences.[64] Second, at the highest photoexcitation fluences, the bands may become filled, which shifts the absorption edge according to the Burstein−Moss effect, and may reduce the absorption coefficient of the GaAs nanowires at the photoexcitation energy, limiting the photoconductivity of the nanowires. The saturation of $-\Delta E/E_{off}$ with increasing fluence places a limit on the modulation depth, extinction, and dynamic range that can be achieved using the simple technique of increasing the pump fluence.

We therefore investigate an alternative means of increasing the modulation depth and extinction ratio, which is to increase the number of layers of parylene-coated GaAs nanowires constituting the polarizer. As the number of layers is increased, there is a rise in the effective areal density of photoexcited nanowires that interact with the THz pulse. Therefore, an increase in the transient THz absorption, that is, in modulation depth, is expected with a larger number of layers. We now characterize the properties of the multilayer THz polarizers consisting of 1, 4, 8, and 14 layers of nanowires embedded in parylene. We note that increasing the number of parylene layers, up to 14 layers is associated with insertion losses of less than 35% across the measurement bandwidth from 0.1 to 4 THz (SI Figure S2).

Figure 3a plots the THz transmission as a function of the optical pump polarization angle for all multilayer samples at the highest fluence investigated (280 μJ cm^{-2}). Similar to the single-layer sample, the THz transmission through the multilayer samples followed the cosine-squared dependence on 2θ described by Malus' law. A large increase in modulation depth and extinction is observed with increasing number of nanowire layers. For the single layer sample, the extinction was less than ∼2%, but the THz modulation becomes more obvious with increasing number of layers with the best performance seen for the 14-layer nanowire sample. The observed increases in extinction, modulation depth, and dynamic range are due to the increased areal density of photoexcited nanowires absorbing THz radiation in the multilayer samples.

We examined the 14-layer nanowire polarizer in further detail, as its behavior can be considered representative of multilayer samples. Figure 4b shows the dependence of THz transmission on the polarization of the pump beam at different photoexcitation fluences. Similar to the single-layer polarizer, the modulation depth increases sublinearly with increasing photoexcitation fluence (SI Figure S3). For the highest fluence of 280 μJ cm^{-2}, the extinction (13.5 ± 1%) was comparable to other graphene and metamaterial-based THz modulators. The modulation depth was measured as −8 dB with a dynamic range of −9 dB. This modulation depth represents a vast improvement over the ultrafast carbon-nanotube based THz polarizer described in previous work.[28]

The temporal dynamics of modulation were measured for all multilayer samples, with Figure 4a plotting the THz trans-

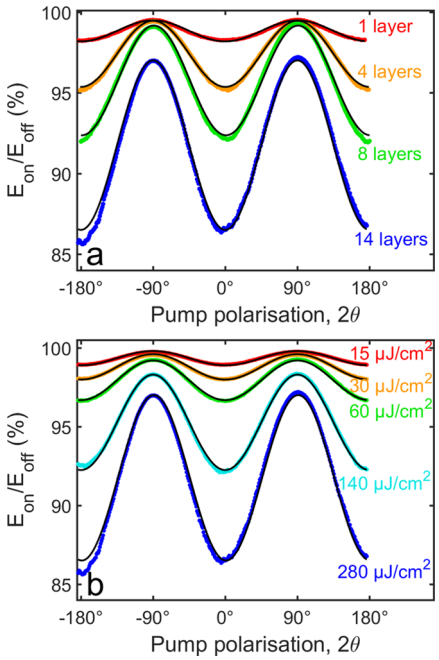

Figure 3. (a) THz transmission, E_{on}/E_{off}, through the photoexcited 1-layer, 4-layer, 8-layer, and 14-layer nanowire polarizers as a function of angle of polarization (2θ) of the photoexcitation pulse with respect to the axis of the nanowires. Solid black lines represent squared-cosine fits, according to Malus' law. (b) THz transmission, E_{on}/E_{off}, through the 14-layer polarizer as a function of angle of polarization (2θ) of the photoexcitation pulse after photoexcitation with pump fluences of 14, 30, 60, 140, and 280 μJ cm^{-2}. Data in panels a and b were measured with the pump−probe delay at t = 0 ps at which $-\Delta E/E_{off}$ is maximum.

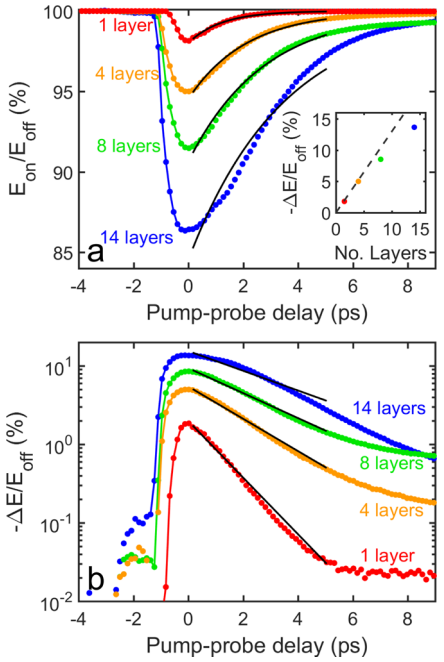

Figure 4. (a) THz transmission, E_{on}/E_{off}, through the photoexcited 1-layer, 4-layer, 8-layer, and 14-layer polarizers as a function of time after photoexcitation. (b) Photoinduced change in transmission, $-\Delta E/E_{off}$, through the same polarizers plotted on a logarithmic ordinate axis. The lines represent single exponential decays fitted to the experimental data, with time constants of 1.2 ps, 2.1 ps, 2.7 ps, and 3.5 ps for the 1-layer, 4-layer, 8-layer, and 14-layer polarizers, respectively. The inset in panel (a) shows the maximum photoinduced change in THz transmission, $\Delta E/E_{off}$, equivalent to modulation depth, as a function of the number of layers constituting the polarizer. All data were taken with the photoexcitation pulse polarized parallel to the nanowire axes (2θ = 0°) and with a photoexcitation pump fluence of 280 μJ cm^{-2}. Data in the inset were measured with the pump−probe delay at t = 0 ps.

DOI: 10.1021/acs.nanolett.7b00401
Nano Lett. 2017, 17, 2603−2610

mission as a function of time after photoexcitation and Figure 4b plotting the photoinduced change in transmission as a function of time after photoexcitation. By fitting monoexponential functions to the data in Figure 4, the decay time constants were extracted for each multilayer sample. The decays were seen to slow with increasing number of nanowire layers, with time constants of 1.1 ± 0.2 ps for the single-layer sample and 3.5 ± 0.3 ps for the 14 layer sample. Slight curvature of the thicker polarizers, and internal reflections due to air gaps unintentionally incorporated between multiple layers, may be responsible for broadening the transient response of the thicker polarizers. Dispersion, whereby the photoexcitation pulse and the THz pulse propagate at slightly different speeds in the polarizer, may also contribute to the observed smearing out of the transient response. The effect of dispersion should, however, be small due to the low thickness (less than 100 μm) of the polarizers. Despite the observed slowing of the transient decay with increasing number of layers, the decay is still on the order of picoseconds even for the thickest 14-layer sample. Therefore, the thickest polarizers maintain picosecond switching speeds while improving modulation depth significantly.

The inset of Figure 4a shows that the modulation depth achieved depends almost linearly on the number of layers constituting the polarizers. There is no obvious saturation of $-\Delta E/E_{off}$ with increasing number of layers up to the maximum number investigated, 14. This result suggests that this type of polarizer could be improved even further by increasing the number of nanowire layers fabricated into the THz polarizer.

The modulation data of Figures 3 and 4 were obtained by measuring the transmission of the peak of the THz pulse. The modulation of the THz peak is broadly representative of the performance of the polarizer across the measurement bandwidth, but analysis of the peak alone does not allow us to assess the frequency-dependence of the modulation. To assess the spectral dependence of the photoinduced modulation and the modulation bandwidth achieved by the 14-layer polarizer across the frequency range from 0.1 to 4 THz, we measured the entire transmitted THz pulse and performed a Fourier analysis. Figure 5 plots the photoinduced change in

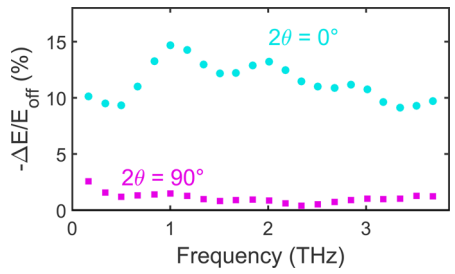

Figure 5. Frequency dependence of the modulation depth, $-\Delta E/E_{off}$, achieved by the 14-layer polarizer. Data were taken with the photoexcitation pulse polarized parallel to the nanowire axes (2θ = 0°, cyan circles) and perpendicular to the nanowire axes (2θ = 90°, magenta squares) with a photoexcitation pump fluence of 280 μJ cm^{-2}.

THz transmission, equivalent to the modulation depth, across the measured frequency range for the cases when the photoexcitation pulse is polarized parallel (2θ = 0°) and perpendicular (2θ = 90°) to the nanowires. When the photoexcitation pulse was polarized perpendicular to the nanowire axis, the photoresponse was minimal throughout the measurement bandwidth. In contrast, when the pump was polarized parallel to the nanowires, strong extinction between 9 and 15% was observed across the entire measurement bandwidth. This indicates that the polarizer has achieved broad bandwidth modulation of the THz transmission.

In summary, we demonstrate for the first time ultrafast THz modulation based on III−V semiconductor nanowire materials. We fabricate THz polarizers from GaAs nanowires embedded in parylene thin films and demonstrate a carrier lifetime of approximately 1 ps, allowing for picosecond switching speeds. We show a broad bandwidth between 0.1 THz and 4 THz for THz transmission through the nanowires, which is the highest bandwidth recorded to date for THz modulation. We also demonstrate that a high extinction of over ∼13% can be obtained by stacking GaAs nanowires embedded in thin parylene films, to give a modulation depth and dynamic range of −8 dB and −9 dB respectively. These values are comparable to those observed for graphene-based THz modulators and surpass those for any previous modulators based on nanostructures, such as unaligned carbon nanotubes. Thus, we highlight semiconductor nanowire-based THz polarizers as ideal candidates for ultrafast THz modulation, as they not only give a large modulation depth, broad bandwidth, and picosecond switching speeds, but also are cheap and easy to manufacture. There is also much scope for further development and improvement of these polarizers. For example, by changing the nanowire electronic characteristics via doping, shell-coating, or wrapping in π-conjugated polymers,[65] the carrier lifetimes and therefore switching speeds can be controlled. Furthermore, the modulation depth and extinction continued to increase almost linearly as the number of layers was increased to 14. This observation suggests that further improvements to this type of multilayer nanowire polarizer will be possible by increasing the number of layers and by improving the nanowire alignment and density further. By utilizing two nanowire polarizers orientated perpendicular to each other, and increasing the number of layers, a modulation depth close to 100% could also be achieved, with THz radiation attenuated in both polarization directions. Thus, we present semiconductor nanowire polarizers as a way of realizing THz intensity and polarization modulation on picosecond time scales, thereby enabling ultrafast THz communication.

■ ASSOCIATED CONTENT

Supporting Information

The Supporting Information is available free of charge on the ACS Publications website at DOI: 10.1021/acs.nanolett.7b00401.

Description of the nanowire growth, sample and experimental geometry, plasmon response, and THz transmission data (PDF)

■ AUTHOR INFORMATION

Corresponding Authors

*E-mail: hannah.joyce@eng.cam.ac.uk.
*E-mail: michael.johnston@physics.ox.ac.uk.

ORCID

Hannah J. Joyce: 0000-0002-9737-680X
Michael B. Johnston: 0000-0002-0301-8033

Author Contributions

⊥S.A.B. and J.L.B. contributed equally.

DOI: 10.1021/acs.nanolett.7b00401
Nano Lett. 2017, 17, 2603−2610

Notes

The authors declare no competing financial interest.

■ ACKNOWLEDGMENTS

The authors thank the EPSRC (U.K.) and Australian Research Council for financial support. H.J.J. thanks the Royal Commission for the Exhibition of 1851 for her research fellowship. The Australian National Fabrication Facility (ACT node) is acknowledged for access to the growth facility used in this work.

■ REFERENCES

(1) Dhillon, S. S.; et al. *J. Phys. D: Appl. Phys.* **2017**, *50*, 043001.
(2) Tonouchi, M. *Nat. Photonics* **2007**, *1*, 97−105.
(3) Ferguson, B.; Zhang, X.-C. *Nat. Mater.* **2002**, *1*, 26−33.
(4) Ulbricht, R.; Hendry, E.; Shan, J.; Heinz, T. F.; Bonn, M. *Rev. Mod. Phys.* **2011**, *83*, 543−586.
(5) Shan, J.; Heinz, T. F. *Ultrafast Dyn. Process. Semicond.* **2004**, *59*, 1−56.
(6) Kress, M.; Löffler, T.; Eden, S.; Thomson, M.; Roskos, H. G. *Opt. Lett.* **2004**, *29*, 1120−1122.
(7) Suto, K.; Nishizawa, J. *Int. J. Infrared Millimeter Waves* **2005**, *26*, 937−952.
(8) Johnston, M. B.; Corchia, A.; Dowd, A.; Linfield, E. H.; Davies, A. G.; McLaughlin, R.; Arnone, D. D.; Pepper, M. *Phys. E* **2002**, *13*, 896−899.
(9) Shen, Y. C.; Upadhya, P. C.; Beere, H. E.; Linfield, E. H.; Davies, A. G.; Gregory, I. S.; Baker, C.; Tribe, W. R.; Evans, M. J. *Appl. Phys. Lett.* **2004**, *85*, 164−166.
(10) Johnston, M. B.; Dowd, A.; Driver, R.; Linfield, E. H.; Davies, A. G.; Whittaker, D. M. *Semicond. Sci. Technol.* **2004**, *19*, S449−S451.
(11) Faist, J.; Capasso, F.; Sivco, D. L.; Sirtori, C.; Hutchinson, A. L.; Cho, A. Y. *Science* **1994**, *264*, 553−556.
(12) Reimann, K. *Rep. Prog. Phys.* **2007**, *70*, 1597−1632.
(13) Nahata, A.; Auston, D. H.; Heinz, T. F.; Wu, C. *Appl. Phys. Lett.* **1996**, *68*, 150−152.
(14) Dai, J.; Liu, J.; Zhang, X. C. *IEEE J. Sel. Top. Quantum Electron.* **2011**, *17*, 183−190.
(15) Cai, Y.; Brener, I.; Lopata, J.; Wynn, J.; Pfeiffer, L.; Stark, J. B.; Wu, Q.; Zhang, X. C.; Federici, J. F. *Appl. Phys. Lett.* **1998**, *73*, 444.
(16) Peng, K.; Parkinson, P.; Fu, L.; Gao, Q.; Jiang, N.; Guo, Y.-N.; Wang, F.; Joyce, H. J.; Boland, J. L.; Tan, H. H.; Jagadish, C.; Johnston, M. B. *Nano Lett.* **2015**, *15*, 206−210.
(17) Peng, K.; Parkinson, P.; Boland, J. L.; Gao, Q.; Wenas, Y. C.; Davies, C. L.; Li, Z.; Fu, L.; Johnston, M. B.; Tan, H. H. *Nano Lett.* **2016**, *16*, 4925−4931.
(18) Boland, J. L.; Conesa-Boj, S.; Parkinson, P.; Tütüncüoglu, G.; Matteini, F.; Rüffer, D.; Casadei, A.; Amaduzzi, F.; Jabeen, F.; Davies, C. L.; Joyce, H. J.; Herz, L. M.; Fontcuberta i Morral, A.; Johnston, M. B. *Nano Lett.* **2015**, *15*, 1336−1342.
(19) Boland, J. L.; Casadei, A.; Matteini, F.; Davies, C. L.; Jabeen, F.; Joyce, H. J.; Herz, L. M.; Fontcuberta, A.; Johnston, M. B. *ACS Nano* **2016**, *10*, 4219−4227.
(20) Beard, M.; Turner, G.; Schmuttenmaer, C. *J. Phys. Chem. A* **2002**, *106*, 6427−6444.
(21) Nahata, A.; Weling, A. S.; Heinz, T. F. *Appl. Phys. Lett.* **1996**, *69*, 2321.
(22) Duvillaret, L.; Garet, F.; Coutaz, J.-L. L. *IEEE J. Sel. Top. Quantum Electron.* **1996**, *2*, 739−746.
(23) Mittleman, D. M.; Gupta, M.; Neelamani, R.; Baraniuk, R. G.; Rudd, J. V.; Koch, M. *Appl. Phys. B: Lasers Opt.* **1999**, *68*, 1085−1094.
(24) Jackson, J. B.; Mourou, M.; Whitaker, J. F.; Duling, I. N.; Williamson, S. L.; Menu, M.; Mourou, G. A. *Opt. Commun.* **2008**, *281*, 527−532.
(25) Shu, J.; Qiu, C.; Astley, V.; Nickel, D.; Mittleman, D. M.; Xu, Q. *Opt. Express* **2011**, *19*, 26666.
(26) Zhang, S.; Zhou, J.; Park, Y.-S.; Rho, J.; Singh, R.; Nam, S.; Azad, A. K.; Chen, H.-T.; Yin, X.; Taylor, A. J.; Zhang, X. *Nat. Commun.* **2012**, *3*, 942.
(27) Grady, N.; Heyes, J. E.; Chowdhury, D. R.; Zeng, Y.; Reiten, M. T.; Azad, A. K.; Taylor, A. J.; Dalvit, D. A. R.; Chen, H.-T. *Science* **2013**, *340*, 1304−1307.
(28) Docherty, C. J.; Stranks, S. D.; Habisreutinger, S. N.; Joyce, H. J.; Herz, L. M.; Nicholas, R. J.; Johnston, M. B. *J. Appl. Phys.* **2014**, *115*, 203108.
(29) Watts, C. M.; Shrekenhamer, D.; Montoya, J.; Lipworth, G.; Hunt, J.; Sleasman, T.; Krishna, S.; Smith, D. R.; Padilla, W. J. *Nat. Photonics* **2014**, *8*, 605−609.
(30) Chan, W. L.; Chen, H. T.; Taylor, A. J.; Brener, I.; Cich, M. J.; Mittleman, D. M. *Appl. Phys. Lett.* **2009**, *94*, 213511.
(31) Kersting, R.; Strasser, K. U. *Electron. Lett.* **2000**, *36*, 1156−1158.
(32) Kleine-Ostmann, T.; Pierz, K.; Hein, G.; Dawson, P.; Marso, M.; Koch, M. *J. Appl. Phys.* **2009**, *105*, 093707.
(33) Hsieh, C.-F.; Lai, Y.-C.; Pan, R.-P.; Pan, C.-L. *Opt. Lett.* **2008**, *33*, 1174−1176.
(34) Hsieh, C.-F.; Pan, R.-P.; Tang, T.-T.; Chen, H.-L.; Pan, C.-L. *Opt. Lett.* **2006**, *31*, 1112−1114.
(35) Yamada, I.; Takano, K.; Hangyo, M.; Saito, M.; Watanabe, W. *Opt. Lett.* **2009**, *34*, 274−276.
(36) Ma, Y.; Khalid, A.; Drysdale, T. D.; Cumming, D. R. S. *Opt. Lett.* **2009**, *34*, 1555−1557.
(37) Li, S.; Yang, Z.; Wang, J.; Zhao, M. *J. Opt. Soc. Am. A* **2011**, *28*, 19−23.
(38) Hochberg, M.; Baehr-Jones, T.; Wang, G.; Shearn, M.; Harvard, K.; Luo, J.; Chen, B.; Shi, Z.; Lawson, R.; Sullivan, P.; Jen, A. K. Y.; Dalton, L.; Scherer, A. *Nat. Mater.* **2006**, *5*, 703−9.
(39) Chen, H. T.; Palit, S.; Tyler, T.; Bingham, C. M.; Zide, J. M. O.; O'Hara, J. F.; Smith, D. R.; Gossard, A. C.; Averitt, R. D.; Padilla, W. J.; Jokerst, N. M.; Taylor, A. J. *Appl. Phys. Lett.* **2008**, *93*, 091117.
(40) Paul, O.; Imhof, C.; Lägel, B.; Wolff, S.; Heinrich, J.; Höfling, S.; Forchel, A.; Zengerle, R.; Beigang, R.; Rahm, M. *Opt. Express* **2009**, *17*, 819−827.
(41) Unlu, M.; Hashemi, M. R.; Berry, C. W.; Li, S.; Yang, S.-H.; Jarrahi, M. *Sci. Rep.* **2014**, *4*, 5708.
(42) Heyes, J. E.; Withayachumnankul, W.; Grady, N. K.; Chowdhury, D. R.; Azad, A. K.; Chen, H. T. *Appl. Phys. Lett.* **2014**, *105*, 181108.
(43) Chen, H.-T.; Padilla, W. J.; Cich, M. J.; Azad, A. K.; Averitt, R. D.; Taylor, A. J. *Nat. Photonics* **2009**, *3*, 148−151.
(44) Mork, J.; Chen, Y.; Heuck, M. *Phys. Rev. Lett.* **2014**, *113*, 1639011.
(45) Born, N.; Scheller, M.; Koch, M.; Moloney, J. V. *Appl. Phys. Lett.* **2014**, *104*, 103508.
(46) Sensale-Rodriguez, B.; Yan, R.; Kelly, M. M.; Fang, T.; Tahy, K.; Hwang, W. S.; Jena, D.; Liu, L.; Xing, H. G. *Nat. Commun.* **2012**, *3*, 780.
(47) Shi, S.; Zeng, B.; Hong, X.; Jung, H. S.; Zettl, A.; Crommie, M. F.; Wang, F. *Nano Lett.* **2015**, *15*, 372−377.
(48) Choi, H. K.; Lee, S. H. S.; Choi, C.-G.; Choi, S.-Y.; Zhang, X.; Choi, M.; Kim, T.-T.; Liu, M.; Yin, X.; Min, B. *Nat. Mater.* **2012**, *11*, 936−941.
(49) Gao, W.; Shu, J.; Reichel, K.; Nickel, D. V.; He, X.; Shi, G.; Vajtai, R.; Ajayan, P. M.; Kono, J.; Mittleman, D. M.; Xu, Q. *Nano Lett.* **2014**, *14*, 1242−1248.
(50) Ren, L.; Pint, C. L.; Booshehri, L. G.; Rice, W. D.; Wang, X.; Hilton, D. J.; Takeya, K.; Kawayama, I.; Tonouchi, M.; Hauge, R. H.; Kono, J. *Nano Lett.* **2009**, *9*, 2610−2613.
(51) Kyoung, J.; Jang, E. Y.; Lima, M. D.; Park, H. R.; Robles, R. O.; Lepro, X.; Kim, Y. H.; Baughman, R. H.; Kim, D. S. *Nano Lett.* **2011**, *11*, 4227−4231.
(52) Karl, N.; Reichel, K.; Chen, H. T.; Taylor, A. J.; Brener, I.; Benz, A.; Reno, J. L.; Mendis, R.; Mittleman, D. M. *Appl. Phys. Lett.* **2014**, *104*, 091115.
(53) Chen, H.-T.; Padilla, W. J.; Zide, J. M. O.; Gossard, A. C.; Taylor, A. J.; Averitt, R. D. *Nature* **2006**, *444*, 597−600.

DOI: 10.1021/acs.nanolett.7b00401
Nano Lett. 2017, 17, 2603−2610

(54) Liu, X.; Parrott, E. P. J.; Ung, B. S.-Y.; Pickwell-MacPherson, E. *APL Photonics* **2016**, *1*, 076103.
(55) Harada, Y.; Ukhtary, M. S.; Wang, M.; Srinivasan, S. K.; Hasdeo, E. H.; Nugraha, A. R. T.; Noe, G. T.; Sakai, Y.; Vajtai, R.; Ajayan, P. M.; Saito, R.; Kono, J. *ACS Photonics* **2017**, *4*, 121−126.
(56) Kang, J.-H.; Gao, Q.; Joyce, H. J.; Tan, H. H.; Jagadish, C.; Kim, Y.; Guo, Y.; Xu, H.; Zou, J.; Fickenscher, M. A.; Smith, L. M.; Jackson, H. E.; Yarrison-Rice, J. M. *Cryst. Growth Des.* **2011**, *11*, 3109−3114.
(57) Joyce, H. J.; Docherty, C. J.; Gao, Q.; Tan, H. H.; Jagadish, C.; Lloyd-Hughes, J.; Herz, L. M.; Johnston, M. B. *Nanotechnology* **2013**, *24*, 214006.
(58) Joyce, H. J.; Boland, J. L.; Davies, C. L.; Baig, S. A.; Johnston, M. B. *Semicond. Sci. Technol.* **2016**, *31*, 103003.
(59) Parkinson, P.; Joyce, H. J.; Gao, Q.; Tan, H. H.; Zhang, X.; Zou, J.; Jagadish, C.; Herz, L. M.; Johnston, M. B. *Nano Lett.* **2009**, *9*, 3349−3353.
(60) Joyce, H. J.; Gao, Q.; Tan, H. H.; Jagadish, C.; Kim, Y.; Zhang, X.; Guo, Y. N.; Zou, J. *Nano Lett.* **2007**, *7*, 921−926.
(61) Gorham, W. F. *J. Polym. Sci., Part A-1: Polym. Chem.* **1966**, *4*, 3027−3039.
(62) Gatesman, A. J.; Waldman, J.; Ji, M.; Musante, C.; Yagvesson, S. *IEEE Microw. Guid. Wave Lett.* **2000**, *10*, 264−266.
(63) Titova, L. V.; Hoang, T. B.; Jackson, H. E.; Smith, L. M.; Yarrison-Rice, J. M.; Kim, Y.; Joyce, H. J.; Tan, H. H.; Jagadish, C. *Appl. Phys. Lett.* **2006**, *89*, 173126.
(64) Joyce, H. J.; Parkinson, P.; Jiang, N.; Docherty, C. J.; Gao, Q.; Tan, H. H.; Jagadish, C.; Herz, L. M.; Johnston, M. B. *Nano Lett.* **2014**, *14*, 5989−94.
(65) Yong, C. K.; Noori, K.; Gao, Q.; Joyce, H. J.; Tan, H. H.; Jagadish, C.; Giustino, F.; Johnston, M. B.; Herz, L. M. *Nano Lett.* **2012**, *12*, 6293−6301.

DOI: 10.1021/acs.nanolett.7b00401
Nano Lett. 2017, 17, 2603−2610